Rational prioritization strategy allows the design of macrolide derivatives that overcome antibiotic resistance

Gerhard König[a,1,2], Pandian Sokkar[a,b,1,3], Niclas Pryk[c,1], Sascha Heinrich[c], David Möller[c], Giuseppe Cimicata[d], Donna Matzov[d], Pascal Dietze[e], Walter Thiel[a,4], Anat Bashan[d], Julia Elisabeth Bandow[e], Johannes Zuegg[f], Ada Yonath[d,5], Frank Schulz[c,5], and Elsa Sanchez-Garcia[a,b,5]

[a]Department of Theory, Max-Planck-Institut für Kohlenforschung, 45470 Mülheim an der Ruhr, Germany; [b]Department of Computational Biochemistry, University of Duisburg-Essen, 45141 Essen, Germany; [c]Fakultät für Chemie und Biochemie, Ruhr-Universität Bochum, 44801 Bochum, Germany; [d]Department of Chemical and Structural Biology, Weizmann Institute, Rehovot 76100 001, Israel; [e]Fakultät für Biologie und Biotechnologie, Ruhr-Universität Bochum, 44801 Bochum, Germany; and [f]Community for Open Antimicrobial Drug Discovery, Institute for Molecular Bioscience, The University of Queensland, Brisbane, QLD 4072, Australia

Edited by Simpson Joseph, University of California San Diego, La Jolla, CA, and accepted by the Editorial Board September 24, 2021 (received for review July 26, 2021)

Antibiotic resistance is a major threat to global health; this problem can be addressed by the development of new antibacterial agents to keep pace with the evolutionary adaptation of pathogens. Computational approaches are essential tools to this end since their application enables fast and early strategical decisions in the drug development process. We present a rational design approach, in which acylide antibiotics were screened based on computational predictions of solubility, membrane permeability, and binding affinity toward the ribosome. To assess our design strategy, we tested all candidates for in vitro inhibitory activity and then evaluated them in vivo with several antibiotic-resistant strains to determine minimal inhibitory concentrations. The predicted best candidate is synthetically more accessible, exhibits higher solubility and binding affinity to the ribosome, and is up to 56 times more active against resistant pathogens than telithromycin. Notably, the best compounds designed by us show activity, especially when combined with the membrane-weakening drug colistin, against *Acinetobacter baumanii*, *Pseudomonas aeruginosa*, and *Escherichia coli*, which are the three most critical targets from the priority list of pathogens of the World Health Organization.

ribosome | QM/MM | antibiotics | resistance | free energy

The resistance of bacterial pathogens against antibiotics is a global problem that requires the constant development of new antibacterial agents (1, 2). The design of new derivatives, based on the modification of existing antibiotics or natural products, relies on extensive structural optimization (3). This process can be time consuming and costly given the possible synthetic routes and the need to consider key factors such as binding affinity, pharmacokinetics, and toxicity. Efficient computational strategies are thus essential to address this problem.

Macrolides are an important class of antibiotics that act against the bacterial ribosome. The first described natural macrolide, erythromycin, is the precursor of semisynthetic modern antibiotics such as azithromycin, clarithromycin, telithromycin, and solithromycin. The design of new macrolide antibiotics commonly relies on semisynthesis and, more recently, on total synthesis (4–11). The synthetic routes comprise 6 linear steps in the case of clarithromycin and 10 or more linear steps for telithromycin or for fully synthetic macrolides. Macrolides bind a conserved position in the bacterial ribosome and only show a small number of polar contacts with ribosomal RNA (12, 13). Crystal structures of bound clarithromycin (14) revealed that the cladinose moiety does not directly interact with the ribosome. Thus, modifications of this side chain can be used to address resistance mechanisms (15–17). As an additional benefit, the cladinose moiety can be replaced by a more synthesizable aryl acetic acid derivative to form acylides (5, 6).

Here, we outline a rational design strategy and apply it to find candidates with improved antibacterial activity based on a prioritization scheme that draws inspiration from branch-and-bound optimization algorithms (18). Candidates are eliminated or prioritized based on theoretical lower and upper bounds for chemical properties that are essential for activity. The protocol provides design decisions as fast and early as possible, aiming for a computational prioritization within a matter of days to guide the synthesis and testing efforts.

Six conditions must be met by a candidate to proceed through the different stages of the prioritization scheme. The molecule must be synthetically accessible (stage I), soluble in aqueous

Significance

Due to the development of resistance against commonly used antibiotics, new derivatives that avoid resistance mechanisms need to be developed. To address this problem, a rational prioritization strategy is outlined for macrolide antibiotics. Candidates are screened based on their solubility, membrane permeability, and binding affinity using a tiered optimization approach of free energy simulations and quantum mechanics/molecular mechanics calculations. After prioritization by computational methods, the best candidates are evaluated experimentally. The strategy creates a targeted substance library that is highly enriched in compounds with antibacterial activity. This allows for faster iterations in the development of new antibiotic derivatives.

Author contributions: G.K., F.S., and E.S.-G. designed research; G.K., P.S., N.P., D. Möller, G.C., D. Matzov, P.D., and A.B. performed research; W.T., A.B., J.E.B., J.Z., and A.Y. contributed new reagents/analytic tools; G.K., P.S., N.P., S.H., A.B., A.Y., F.S., and E.S.-G. analyzed data; and G.K., P.S., F.S., and E.S.-G. wrote the paper.

The authors declare no competing interest.

This article is a PNAS Direct Submission. S.J. is a guest editor invited by the Editorial Board.

[1]G.K., P.S., and N.P. contributed equally to this work.

[2]Present address: Centre for Enzyme Innovation, School of Biological Sciences, University of Portsmouth, PO1 2DT Portsmouth, United Kingdom.

[3]Present address: Faculty of Allied Health Sciences, Chettinad Hospital and Research Institute, Chettinad Academy of Research and Education, Kelambakkam 603103, India.

[4]Deceased August 23, 2019.

[5]To whom correspondence may be addressed. Email: ada.yonath@weizmann.ac.il, frank.schulz@ruhr-uni-bochum.de, or elsa.sanchez-garcia@uni-due.de.

This article contains supporting information online at https://www.pnas.org/lookup/suppl/doi:10.1073/pnas.2113632118/-/DCSupplemental.

Published November 8, 2021.

solution (stage IIa), and exhibit sufficient membrane permeability (stage IIb) as well as high binding affinity toward the target (stages IIIa to IIId). Moreover, candidates should avoid resistance mechanisms (stage IV) and must be nontoxic (stage V). The design process is simplified when the optimization starts from an approved drug since therapeutic agents generally fulfill most of these conditions. Thus, the focus lies on eliminating modifications that lead to a loss of essential properties and on favoring candidates for which these properties are improved or at least conserved. From one stage to the next, fewer molecules are evaluated but with increasing rigor. The rational design starts with a strategy for synthesis, followed by prioritization through a series of computational techniques. The prioritized molecules are then tested both in vitro and in vivo. The toxicity of the most active candidates is evaluated in the final stage.

In this work, we validate our design strategy with the study of 19 acylide replacements of the cladinose moiety of clarithromycin using four linear synthesis steps (Fig. 1). This is two steps shorter than that for telithromycin. The numbering of the library starts with the original clarithromycin molecule (**1**; CTY). Its derivatives include substituents with different polarities and electron densities, aliphatic analogs, or inflexible spacers between the macrolide core and the aryl substituent. The set was designed to evaluate the effects of nitro substituents (5, 6), an extended π system, an electron-donating substituent, and a cyclohexyl derivative (as a nonaromatic comparison), as well as halogenated and methylated derivatives. Both the spatial and electronic constraints on the scaffold are explored.

Results

All computational results are derived from a consistent set of relative free energy perturbation (FEP) simulations. The ligands were simulated both in the unbound state in aqueous solution and in the bound state within the bacterial ribosome. The bound states of clarithromycin and the acylide derivatives were modeled with the structure of the 50S ribosome of *Deinococcus radiodurans* together with explicit water and with an ionic concentration of 0.1 M. The clarithromycin–ribosome complex was equilibrated with molecular dynamics simulations (*SI Appendix*, section A and Fig. S1). In parallel, relative FEP protocols for all ligands were set up and tested in aqueous solution. The simulations decouple the side chains of the acylides as shown in Fig. 1, leaving only the common backbone as the alchemical intermediate state. This also allows the use of enhanced sampling methods for exploring the conformational flexibility of the side chains (19).

First, we estimated the relative affinities for water, in the absence of the ribosome, using implicit solvent calculations (stage IIa) (*SI Appendix*, section C) (20). These calculations represent an upper bound for their relative solubilities and neglect self-solvation effects (21), as well as the free energy of sublimation (22). Stage IIa was motivated by the relatively poor solubility of clarithromycin and the assumption that hydrophilic molecules might be less affected by promiscuous adenosine triphosphate (ATP)–dependent efflux pumps (17, 23). Since all molecules were predicted to be more hydrophilic than clarithromycin (*SI Appendix*, Table S1), we used the five compounds with the highest affinity for water (**6**, **3**, **8**, **5**, **4**) for the next stage (stage III, where we calculated the binding free energy of the ligands toward the ribosome).

Likewise, we estimated membrane permeabilities using an implicit membrane model (stage IIb) (*SI Appendix*, section C) (24). The resulting transfer free energies gauge membrane permeability based on Fick's First Law (25) but neglect self-solvation effects (26), as well as the nanostructure of the membrane. Since all candidates were considered to be membrane permeable

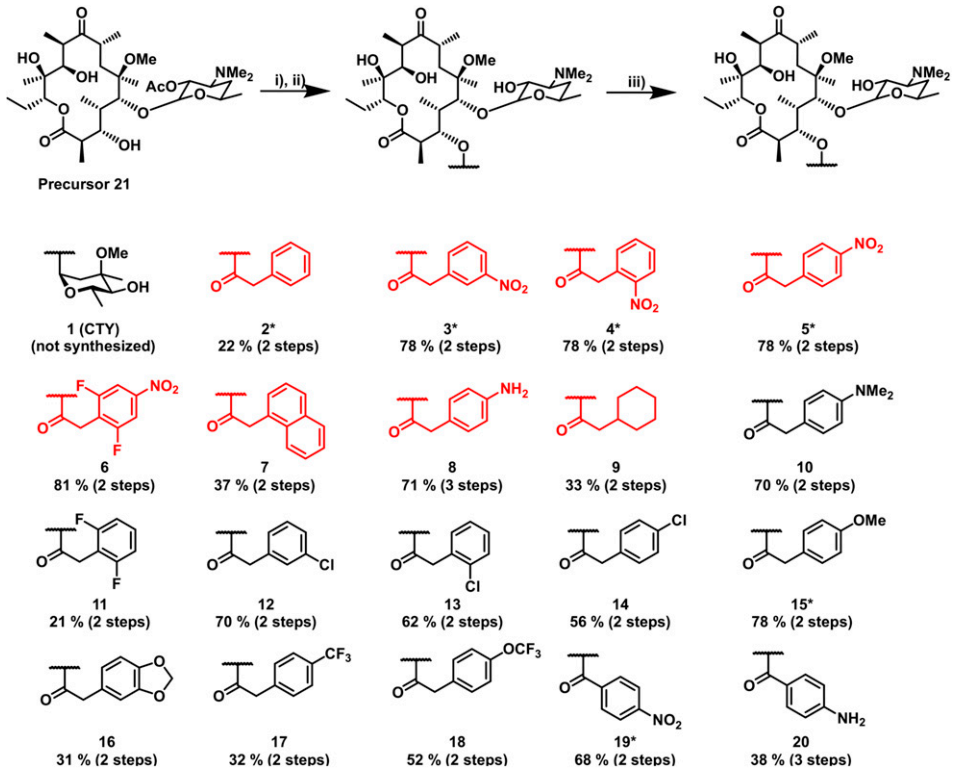

Fig. 1. Synthesis of the acylide library. CTY denotes clarithromycin. (*i*) 6.1 eq. $ArCH_2CO_2H$, 6.0 eq. 1-ethyl-3-(3-dimethylaminopropyl)carbodiimide· HCl, 1.1 eq. 4-dimethylaminopyridine (DMAP), dichloromethane (DCM), room temperature or 3.3 eq. $ArCH_2CO_2H$, 3.3 eq. trimethylacetyl chloride, 3.3 eq. Et_3N, 1 eq. DMAP, DCM, -15° C $\rightarrow$ RT. (*ii*) MeOH, RT, 48 h. (*iii*) 2 eq. $NiCl_2 \cdot 6H_2O$, 4 eq. $NaBH_4$, MeOH, 0° C. Computed structures are highlighted in red. *Previously described compounds.

(*SI Appendix*, Table S2), the five molecules with the highest affinity for the cell membrane (**7**, **2**, **9**, **18**, **14**) were also prioritized for the binding free energy calculations in stage III. Stage IIb was motivated by the assumption that membrane-permeable molecules are more likely to enter bacterial cells (17).

Accordingly, we selected molecules **2** to **9**, **14**, and **18** for FEP binding free calculations (stage III). The final frame from the molecular dynamics simulations of **1** bound to the ribosome served as the starting point for relative FEP calculations of the bound state (*SI Appendix*, section D). To reduce computational costs, the ribosome was truncated to a subsystem comprising 0.1 million atoms, and all atoms outside of the binding pocket were kept frozen. Thus, any slow structural transitions of the ribosome are neglected.

The equilibration phase of the FEP binding simulations was employed to filter out nonbinders by postprocessing the trajectories of compounds **2** to **9**, **14**, and **18** with molecular mechanics energies combined with generalized Born and surface area (MM-GBSA) continuum solvation calculations based on one trajectory (stage IIIa) (*SI Appendix*, section D) (27, 28). These types of calculations only provide very approximate estimations of the free energy changes since the structural relaxation of the unbound state is not accounted for and due to the implicit treatment of the solvent. In addition, any slow relaxation of the binding pocket is neglected due to the short simulation length. Nevertheless, this step allowed us to eliminate compounds **14** and **18** because they exhibited highly unfavorable relative binding free energies (*SI Appendix*, Table S3).

Next, we calculated the relative free energies of binding ($\Delta\Delta G_{bind}$) and relative free energies of hydration ($\Delta\Delta G_{hydr}$) of the remaining prioritized set of compounds (**2** to **9**) with respect to clarithromycin using a rigorous free energy estimator and explicit solvent (stage IIIb) (Table 1 and *SI Appendix*, section B). Based on similar FEP protocols in the blind Statistical Assessment of the Modeling of Proteins and Ligands (SAMPL) prediction challenges (29, 30), the expected error of these calculations is between 2 and 3 kcal mol^{-1}. Thus, molecule **6** is a significantly better binder than clarithromycin, while molecules **3**, **4**, **5**, and possibly **9** are likely to exhibit improved binding affinities toward the ribosome. The explicit solvent $\Delta\Delta G_{hydr}$ values confirm that all tested compounds are more hydrophilic than clarithromycin, especially **6**.

In stage IIIc, we carried out quantum mechanics/molecular mechanics (QM/MM) calculations to further explore the relative stability of the ribosome–ligand complexes in explicit solvent (*SI Appendix*, section E). The relative average interaction energies of the ligands with their surroundings were determined in the ribosome ($\Delta\Delta E_{ribo}$) and in aqueous solution ($\Delta\Delta E_{aq}$). The use of QM/MM approaches previously improved the accuracy of computational free energy predictions by about 1 kcal mol^{-1} (30, 31). The QM/MM calculations indicate that compounds **6**, **5**, and **4** exhibit the most favorable interaction energies with the ribosome. They were, therefore, prioritized for the in vitro testing (stage IIId). Molecules **7** and **8** were eliminated because of the predicted instability of their complexes with the ribosome (Table 1). The results for the other molecules are less clear, as stronger interactions with the ribosome are often offset by a simultaneous high affinity for the unbound state in water. Overall, the QM/MM interaction energies confirm the FEP results, indicating that **6** is a very favorable binder to the ribosome. In addition, ligands **5** and **4** emerge as potential effective inhibitors. A detailed discussion of the simulations of the ligand–ribosome complexes is provided in *SI Appendix*, section E.

Table 1. Computed relative binding free energies ($\Delta\Delta G_{bind}$) and relative hydration free energies ($\Delta\Delta G_{hydr}$), as well as average QM/MM interaction energies in the ribosome ($\Delta\Delta E_{ribo}$) and in aqueous solution ($\Delta\Delta E_{aq}$) for the prioritized acylides with respect to clarithromycin (in kilocalories mole^{-1})

Ligand	$\Delta\Delta G_{bind}$	$\Delta\Delta G_{hydr}$	$\Delta\Delta E_{ribo}$	$\Delta\Delta E_{aq}$
6*	–4.3 ± 1.5	–8.5 ± 0.9	–38.8 ± 0.3	–15.3 ± 0.6
5*	–2.0 ± 1.5	–4.9 ± 0.9	–34.6 ± 0.3	–23.5 ± 0.6
4*	–2.5 ± 1.5	–1.9 ± 1.0	–27.5 ± 0.3	–4.3 ± 0.6
3	–2.4 ± 1.5	–4.2 ± 1.0	–11.5 ± 0.3	–22.0 ± 0.6
2	–0.3 ± 1.5	–3.0 ± 0.9	–6.4 ± 0.3	3.9 ± 0.6
9	–1.9 ± 1.5	–2.7 ± 0.9	–2.7 ± 0.3	–3.2 ± 0.6
8	5.8 ± 1.5	–3.1 ± 1.0	0.8 ± 0.3	–8.7 ± 0.6
7	12.2 ± 1.6	–3.4 ± 0.9	11.3 ± 0.3	5.4 ± 0.6

The molecules are ordered based on their QM/MM affinity toward the ribosome.
*The three best candidates.

To evaluate our rational design strategy, the inhibitory activities of all 19 candidates were determined by the half maximal inhibitory concentrations (IC_{50}) from an in vitro transcription–translation assay against the *Escherichia coli* ribosome (stage IIId) (*SI Appendix*, part 2). As evidenced in Fig. 2, compounds **6** and **4** are indeed the most active in the whole set, and **5** is more active than clarithromycin. Molecule **7**, which was predicted to be the worst binder in the prioritized set, also turns out the be the least active in this subset. Ligands **11**, **13**, **15**, and **16** also show high affinity toward the ribosome but were not part of the prioritized set because of their solvation properties. Membrane permeability and hydrophobicity are expected to play a prominent role for biological activity.

In stage IV, we tested the acylides for in vitro antimicrobial activity by assessing minimal inhibitory concentrations (MICs) against gram-positive bacteria (*Bacillus subtilis* and *Staphylococcus aureus*) as well as against gram-negative bacteria (*E. coli*, *Acinetobacter baumanii*, *Pseudomonas aeruginosa*, and *Klebsiella pneumoniae*) and yeast strains (*Candida albicans* and *Cryptococcus neoformans*). The MIC results are listed in Fig. 3. We also tested the cytotoxicity and hemolytic activity by assessing cytotoxic concentration (CC_{50}) against the human kidney cell line HEK293 and hemolytic concentration (HC_{10}) against human red blood cells (stage V) (the last two rows of Fig. 3). For MIC values up to 32 μg mL^{-1}, therapeutic indices are calculated (CC_{50}/MIC) and shown in parentheses below the respective MIC value in Fig. 3. As the ester bond in acylides might be prone to enzymatic breakdown, all acylides were tested to be stable in human blood serum (32).

All compounds are highly active against the methicillin-susceptible strain of *S. aureus* (MSSA, *DSM 20231*, *ATCC 12600*)

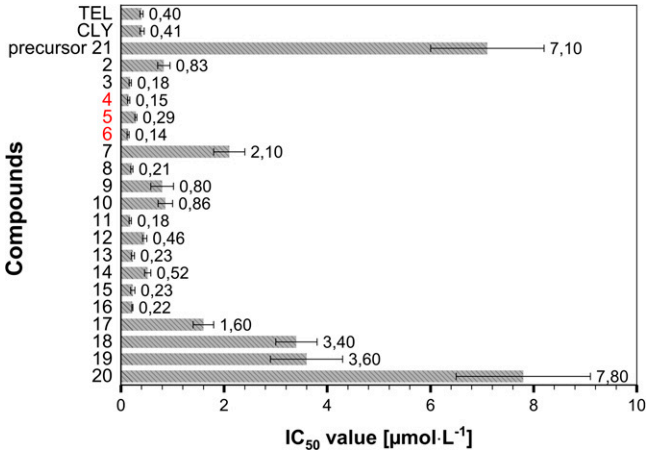

Fig. 2. IC_{50} data for the inhibition of the *E. coli* ribosome by telithromycin (TEL), clarithromycin (CLY), the precursor molecule (**21**), and all 19 candidates. The three best candidates from the computational preselection are highlighted in red.

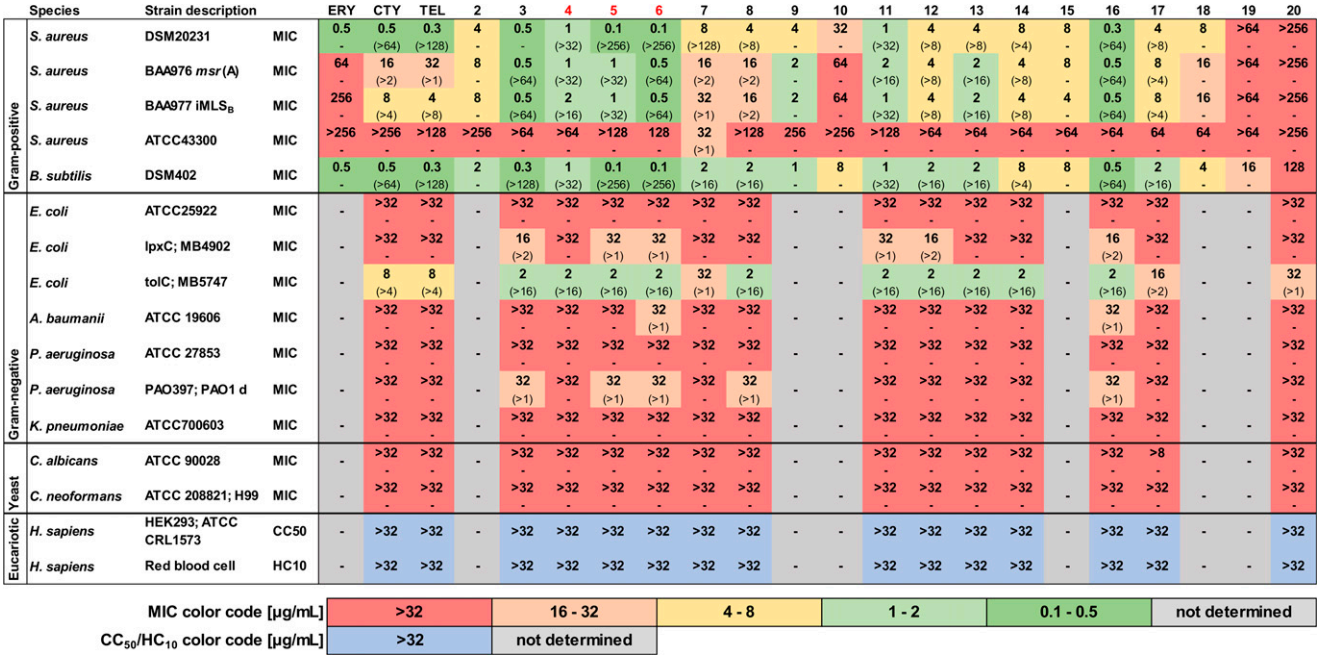

Fig. 3. Activity against a variety of gram-negative strains and yeast, the gram-positive bacteria *B. subtilis*, and the high-priority pathogen *S. aureus* (32). MICs are given for erythromycin (ERY), clarithromycin (CTY), telithromycin (TEL), and all candidates. The three best candidates from the computational stage (**4** to **6**) are highlighted in red. Additionally, CC_{50} (*Homo sapiens HEK293*) and HC_{10} (*H. sapiens* red blood cells) values are provided. Selectivity indices (CC_{50} value divided by MIC) are shown in parentheses below the respective MIC value. The selectivity indices are color coded together with the respective MIC value to facilitate readability. Not determined values are indicated by a dash.

(33) with MIC values up to $0.1\,\mu g\,mL^{-1}$ while displaying no cytotoxicity or hemolytic activity at the same concentrations, as well as no activity against either of the yeast strains. Exceptions are only compounds **19** and **20**, the two benzoic acid variants, which have no antibacterial activity. The high antibiotic activity of the other compounds is retained against *B. subtilis* (*DSM 402*, *NCIB 10106*) and mostly against two mutant strains of MSSA: *S. aureus BAA-976* and *BA-977*. *S. aureus BAA 977* features inducible macrolide–lincosamide–streptogramin B resistance due to the erythromycin ribosomal methylase *erm(C)* gene that alters the ribosomal structure (34), while *S. aureus BAA 976* is macrolide resistant due to the ATP-dependent efflux pump associated with the *msr(A)* gene. Both strains display resistance against the reference antibiotics erythromycin, clarithromycin, and telithromycin. Most compounds retain similar activity in the resistant strains compared with the MSSA strains. The only exceptions are compound **5**, which displays a 10-fold reduction of activity (MIC value shift from 0.1 to $1\,\mu g\,mL^{-1}$); compound **6** with a 5-fold reduction (MIC value shift from 0.1 to $0.5\,\mu g\,mL^{-1}$); and compound **8** with a 4-fold reduction (MIC value shift from 4 to $16\,\mu g\,mL^{-1}$). Compounds **3**, **6**, and **16** still retain a high antibiotic activity with MIC values $< 1\,\mu g\,mL^{-1}$ in the resistant strains.

None of the compounds show high activity against the MRSA strain *S. aureus ATCC 43300*, which harbors, among other resistant genes, the *erm(A)* gene. The only notable exception is compound **7**, for which an MIC value of $32\,\mu g\,mL^{-1}$ was measured. The same compound showed only moderate activity compared to the other strains tested. This may be related to structural rearrangements in the binding pocket, caused by the bulky side chain of **7**, that mitigate the effect of RNA methylation on the binding affinity.

Next, antibacterial MIC data were determined against several gram-negative pathogens, including type strains from *A. baumanii* (*DSM 30007*, *ATCC 19606*), *P. aeruginosa* (*DSM 50071*, and *ATCC 27853*), *E. coli* (*DSM 30083*, *ATCC 11775*, and *ATCC 25922*), and *K. pneumoniae* (*ATCC 700603*) (Fig. 3 and Table 2). Those four species are the top-ranked bacteria from the World Health Organization (WHO) priority pathogens list for the development of new antibiotics (33). Similar to established macrolide antibiotics, most compounds display no activity against the panel of gram-negative bacteria. A notable exception is once more compound **6**, showing activity against *A. baumannii* (MIC between 8 and $32\,\mu g\,mL^{-1}$). To a lesser degree, compounds **11** (MIC of $64\,\mu g\,mL^{-1}$) and **16** (MIC between 16 and $32\,\mu g\,mL^{-1}$) are also active.

In addition, the compounds were tested against gram-negative strains that harbor mutations, which affect the drug permeability through the bacterial membrane, including *E.*

Table 2. Activity against the three top-ranked bacteria from the WHO priority pathogens list (33)

	MIC ($\mu mol\ L^{-1}$)		
	A. baumanii DSM 30007	*P. aeruginosa DSM 50071*	*E. coli DSM 30083*
COS	0.125	0.5	0.125
6*	8.0	> 128	128.0
6* + COS (0.1 × MIC)	0.25	> 128	32.0
6* + COS (0.5 × MIC)	0.25	16.0	0.5
11	64	> 128	64
11 + COS (0.1 × MIC)	1	> 128	64
11 + COS (0.5 × MIC)	0.25	64	2
16	16	> 64	> 64
16 + COS (0.1 × MIC)	0.25	> 64	16
16 + COS (0.5 × MIC)	0.125	32	0.25

MICs are given for molecules **6**, **11**, and **16** in combination with subinhibitory concentrations of the membrane-weakening antibiotic colistin sulfate (COS). Erythromycin, clarithromycin, telithromycin, and all other acylides were ineffective.
*Best candidate.

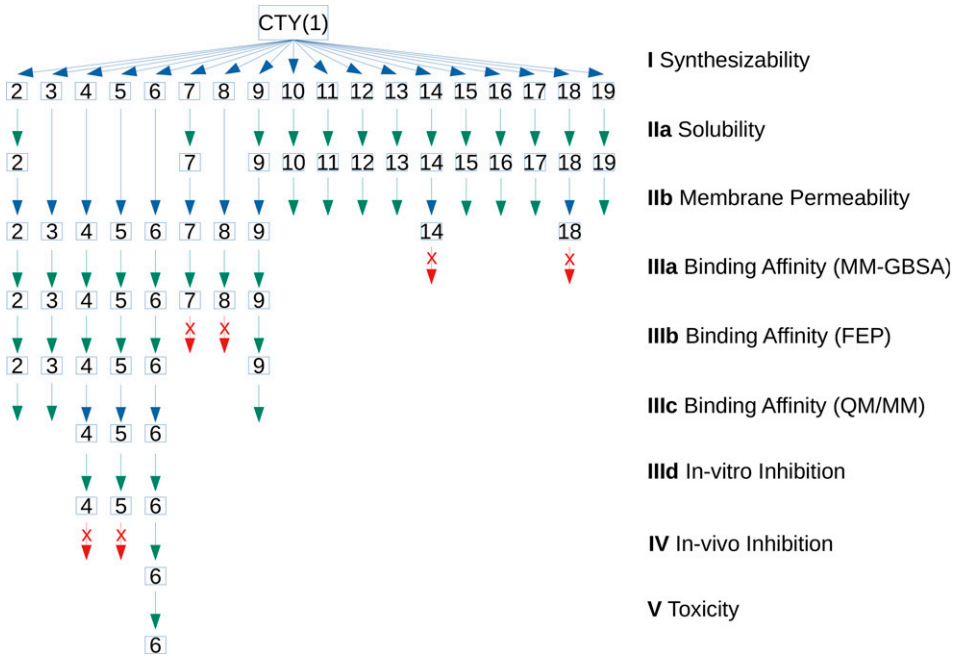

Fig. 4. The decision-making process in the outlined rational design scheme. Each derivative of clarithromycin (CTY) must pass tests for synthesizability, solubility, membrane permeability, binding affinity at three different levels of accuracy (short MM-GBSA calculations, FEP simulations, and QM/MM calculations), in vitro inhibition of the ribosome, in vivo inhibition of resistant bacterial strains, and toxicity. Green arrows indicate molecules that meet the criteria and can be considered for further testing at the next level. Blue arrows indicate prioritization of molecules with especially beneficial properties. Crossed-out red arrows indicate molecules that have been eliminated because they significantly lack essential properties. The different levels of testing are ordered based on their (computational) expenses. The prioritization of molecules considers both the likelihood of exhibiting high activity and the available resources. Hypothetically, if all prioritized molecules fail to pass the test at one stage, the search should backtrack and continue with molecules with green arrows at a previous level until either a suitable drug candidate has been found or all options have been exhausted.

coli Δ *lpxC* (variation of the lipopolysaccharide structure) and Δ *tolC* (without the major efflux pump) and *P. aeruginosa* Δ *mexAB/CD/EF/JKL/XY* (without five of the major efflux pumps). Interestingly, all compounds regain significant activity (up to MIC values of 2 $\mu g\,mL^{-1}$) if the major drug efflux pump is eliminated in *E. coli*. This also includes compound **20**, which is otherwise not even active against gram-positive bacteria. Variation of the outer membrane by Δ *lpxC* had a lesser effect, with only compounds **3**, **5**, **6**, **11**, **12**, and **16** regaining activity to MIC values of 16 to 32 $\mu g\,mL^{-1}$. A similarly small effect was displayed for the *P. aeruginosa* strain that lacks five of the major drug efflux pumps. Only five compounds regain activity to MIC values of 32 $\mu g\,mL^{-1}$ (Fig. 3).

A similar outcome can be achieved by the coadministration of sub-MIC levels of colistin, an antibiotic that interacts with the outer membrane component Lipid A, thereby increasing the permeability of the membrane for other drugs. Colistin showed synergistic activity with each of the tested acylides **6**, **11**, and **16** against *E. coli* and *A. baumanii*, increasing the activity to MIC values of 0.25 to 1 $\mu g\,mL^{-1}$, at colistin concentrations of 10% of its MIC value (Table 2). Like the efflux pump mutants, activity with colistin against *P. aeruginosa* could not be reestablished to the same degree as for *E. coli* or *A. baumanii*, suggesting that *P. aeruginosa* still has effective efflux mechanisms. The activity against the efflux-deficient *E. coli* Δ *tolC* mutant suggests that the main cause of the resistance in gram-negative bacteria is the efficient elimination of the compounds via efflux pumps. In addition, the activities against *E. coli* Δ *tolC* agree with the IC_{50} values, with most MIC values around 2 $\mu g\,mL^{-1}$ and IC_{50} values $< 0.5\,\mu M$. Exceptions are the weaker binders **7**, **17**, and **20**, which also display IC_{50} values above 1 μM and MIC values at 16 to 32 $\mu g\,mL^{-1}$. This suggests that the activity against *S. aureus*, which exhibits a wider range of MIC values, might be governed by permeability as well.

Discussion and Conclusions

Our rational design strategy allowed us to successfully reduce the library of 19 derivatives of clarithromycin first to 10 and then to 3 candidates (**6**, **4**, **5**) by calculating solubilities, membrane permeabilities, and binding affinities at three different levels of accuracy (end point methods with implicit solvent, FEP with explicit solvent, and QM/MM calculations). In vitro experiments confirmed that molecules **6** and **4** exhibit the lowest IC_{50} of the whole set. The heuristic prioritization process allows fast and early decisions based on several approximations. In theory, only three molecules had to be synthesized and tested to find the best candidate (**6**). An overview of the decision-making process is provided in Fig. 4.

Compounds **6**, **16**, and **11** exhibited some activity against the top three critical targets from the WHO priority pathogens list (32). Further experiments demonstrated that *A. baumanii* and *E. coli* can be successfully inhibited by these compounds in combination with the membrane-weakening compound colistin or by elimination of the major efflux pump system. This confirms that the uptake through the outer membrane is a limiting factor in gram-negative bacteria. In addition, the comparison with the membrane-deficient *E. coli* and MSSA *S. aureus* strain suggests that, even in gram-positive bacteria, permeability through the membrane affects the activity.

In vitro activity data for the high-priority pathogen *S. aureus* allowed us to identify molecules **6**, **3**, and **16** as the most promising candidates with high activity, no cytotoxicity, and the ability to overcome existing macrolide resistance. Compared with telithromycin, lead compound **6** exhibits a 56-fold higher activity against *S. aureus BAA 976* and an 8-fold increased activity against *S. aureus BAA 977*. Both activities are below the European Committee on Antimicrobial Susceptibility Testing (EUCAST) clinical break point of 1 $\mu g\,mL^{-1}$ (35), which makes the molecule

a good candidate to break the macrolide resistance in *S. aureus*. The comparison between the biophysical IC_{50} data (Fig. 2) and cell-based MIC data (Fig. 3) indicates a good correlation for gram-negative bacteria where the major efflux pump has been deactivated (*E. coli* Δ *tolC*). Nevertheless, several discrepancies can be observed for compounds with similar potencies in gram-positive wild-type strains, like *S. aureus*. This suggests different uptake rates in gram-positive bacteria. Compounds **6**, **3**, and **16** exhibit good MIC values.

The experimental data allow us to evaluate the design decisions, showing that an efficient strategy must account for more criteria than just binding affinity. Among the prioritized molecules in Table 1, the QM/MM calculations identified 80% of the active compounds in terms of IC_{50}, and 67% of the predictions were correct (*SI Appendix*, Fig. S11). Strikingly, not a single molecule that was prioritized because of its high membrane permeability (**2**, **7**, **14**, **18**, and to a lesser degree, **9**) turned out to be effective. In contrast, almost all molecules that were selected for their hydrophilicity (**3**, **4**, **5**, **6**, and to a lesser degree, **8**) were more active than clarithromycin. Thus, hydrophilicity turned out to be the better design criterion than high membrane permeability to reach low MIC values.

Some active compounds (in particular, molecules **16** and to some degree, also **11**) were missed in the initial stages of the selection process. Molecule **16** almost progressed further, being among the six most hydrophilic molecules. However, MM-GBSA calculations predicted a low binding affinity for **16** (*SI Appendix*, Table S3). Compound **11** was given a low priority because it ranked low in terms of both hydrophilicity and membrane permeability. It also would have exhibited a poor binding affinity in a posteriori MM-GBSA calculations (*SI Appendix*, Table S3). Thus, it did not meet any of the considered requirements.

Any rational design scheme can only be as good as its design criteria. Future prioritization schemes could benefit from a better understanding of antibacterial activity against wild-type and efflux pump mutants, as well as other resistance mechanisms. A weighted scoring function that identifies the most important physicochemical traits and their contributions to uptake and activity could guide the rational design process. Theoretical bounds with improved convergence properties could speed up the computational prioritization scheme. Additional in silico steps to evaluate the binding affinity of the compounds against different ribosome strains should be the next stage in the development of rational design strategies.

Materials and Methods

The simulations were carried out using the CHARMM (36, 37) and NAMD (38) programs with the CHARMM36 force field (39–41). The large ribosomal subunit (50S) from *D. radiodurans* (Protein Data Bank ID codes 2ZJR and 1J5A) (13, 14, 42) and all Mg^{2+} ions from the crystal structures were solvated in a cubic box with 0.1 M KCl. The box size was equilibrated with constant pressure simulations, and 20 ns of molecular dynamics simulations were performed. The free energy simulations and QM/MM calculations are based on 5ns simulations with Hamiltonian replica exchange (43, 44) of a truncated ribosome model. The free energy differences were analyzed with the FREN module of CHARMM (45, 46). The implicit solvent calculations of solubility (21, 30), membrane permeability (25), and MM-GBSA binding affinity (27, 28) were conducted with the GBMV implicit solvent model (20, 24). The QM/MM calculations were performed with the ChemShell package (47) using the MNDO program (48) for the semiempirical calculations with OM2-D3 (49–51), Turbomole (52) for the QM calculations with BP86-D3/Def2-SVP (53, 54), and DL_POLY (55) for the MM calculations (56).

For the experimental testing, the compounds were synthesized as indicated in Fig. 1. The compounds were subjected to an IC_{50} determination assay against the *E. coli* ribosome. Cell lysates were prepared as described previously (57). Luminescence measurements were carried out on a Labtech Clariostar microtiter plate reader. The stability of acylides in human blood plasma has been investigated as described before (33). The determination of the MICs and the cytotoxicity data was carried out as outlined in refs. 58 and 59.

Detailed computational (*SI Appendix*, part 1) and experimental methodologies (*SI Appendix*, part 2) (containing synthetic procedures, IC_{50} determination, MIC determinations, cytotoxicity determination, KIT ComPlat IDs for most of the final compounds, and further detailed information) are available in *SI Appendix*.

Data Availability. All study data are included in the article and/or *SI Appendix*.

ACKNOWLEDGMENTS. This work was supported by the German Research Foundation (DFG) under Germany's Excellence Strategy EXC 2033–390677874–RESOLV. P.S. and E.S.-G. acknowledge the Gauss Centre for Supercomputing e.V. (GCS; https://www.gauss-centre.eu) for funding this project by providing computing time on the GCS Supercomputer JUQUEEN at Jülich Supercomputing Centre. J.E.B. acknowledges funding from the Federal State of North Rhine-Westphalia and the European Regional Development Fund for the Research Infrastructure "Center for Systembased Antibiotic Research." A.Y. was supported by European Research Council Grant 322581 "Novel Insights into Multi-Drug Resistance to Antibiotics and the Primordial Ribosome" and the Kimmelman Center for Macromolecular Assemblies; additionally, A.Y. holds the Martin S. and Helen Kimmel Professorial Chair at the Weizmann Institute of Science. F.S. was funded by DFG Research Training Group GRK 2341 "Microbial Substrate Conversion." E.S.-G. acknowledges the support of the Boehringer Ingelheim Foundation (Plus-3 Program) and of the Collaborative Research Center 1093 "Supramolecular Chemistry on Proteins" funded by the DFG.

1. J. Hopwood, A call to arms. *Nat. Rev. Drug Discov.* **6**, 8–12 (2007).
2. C. L. Ventola, The antibiotic resistance crisis. Part 1: Causes and threats. *P&T* **40**, 277–283 (2015).
3. D. J. Newman, G. M. Cragg, Drugs and drug candidates from marine sources: An assessment of the current "state of play." *Planta Med.* **82**, 775–789 (2016).
4. I. B. Seiple *et al.*, A platform for the discovery of new macrolide antibiotics. *Nature* **533**, 338–345 (2016).
5. T. Tanikawa *et al.*, Synthesis and antibacterial activity of acylides (3-O-acylerythromycin derivatives): A novel class of macrolide antibiotics. *J. Med. Chem.* **44**, 4027–4030 (2001).
6. T. Tanikawa *et al.*, Synthesis and antibacterial activity of a novel series of acylides: 3-O-(3-pyridyl)acetylerythromycin A derivatives. *J. Med. Chem.* **46**, 2706–2715 (2003).
7. C. H. Ballow, G. W. Amsden, Azithromycin: The first azalide antibiotic. *Ann. Pharmacother.* **26**, 1253–1261 (1992).
8. H. E. Kaufman, Spiramycin. *Arch. Ophthalmol.* **66**, 609–610 (1961).
9. S. K. Puri, H. B. Lassman, Roxithromycin: A pharmacokinetic review of a macrolide. *J. Antimicrob. Chemother.* **20** (suppl. B), 89–100 (1987).
10. Y. Watanabe, S. Morimoto, T. Adachi, M. Kashimura, T. Asaka, Chemical modification of erythromycins. IX. Selective methylation at the C-6 hydroxyl group of erythromycin A oxime derivatives and preparation of clarithromycin. *J. Antibiot. (Tokyo)* **46**, 647–660 (1993).
11. A. Denis *et al.*, Synthesis and antibacterial activity of HMR 3647 a new ketolide highly potent against erythromycin-resistant and susceptible pathogens. *Bioorg. Med. Chem. Lett.* **9**, 3075–3080 (1999).
12. J. A. Dunkle, L. Xiong, A. S. Mankin, J. H. Cate, Structures of the *Escherichia coli* ribosome with antibiotics bound near the peptidyl transferase center explain spectra of drug action. *Proc. Natl. Acad. Sci. U.S.A.* **107**, 17152–17157 (2010).
13. J. M. Harms *et al.*, Translational regulation via L11: Molecular switches on the ribosome turned on and off by thiostrepton and micrococcin. *Mol. Cell* **30**, 26–38 (2008).
14. F. Schlünzen *et al.*, Structural basis for the interaction of antibiotics with the peptidyl transferase centre in eubacteria. *Nature* **413**, 814–821 (2001).
15. M. F. Chellat, L. Raguž, R. Riedl, Targeting antibiotic resistance. *Angew. Chem. Int. Ed. Engl.* **55**, 6600–6626 (2016).
16. A. L. Prunier, B. Malbruny, D. Tandé, B. Picard, R. Leclercq, Clinical isolates of *Staphylococcus aureus* with ribosomal mutations conferring resistance to macrolides. *Antimicrob. Agents Chemother.* **46**, 3054–3056 (2002).
17. A. Kumar, H. P. Schweizer, Bacterial resistance to antibiotics: Active efflux and reduced uptake. *Adv. Drug Deliv. Rev.* **57**, 1486–1513 (2005).
18. A. Przybylski, X. Gandibleux, Multi-objective branch and bound. *Eur. J. Oper. Res.* **260**, 856–872 (2017).
19. D. F. Hahn, G. König, P. H. Hünenberger, Overcoming orthogonal barriers in alchemical free energy calculations: On the relative merits of λ-variations, λ-extrapolations, and biasing. *J. Chem. Theory Comput.* **16**, 1630–1645 (2020).
20. M. S. Lee, M. Feig, F. R. Salsbury Jr., C. L. Brooks III, New analytic approximation to the standard molecular volume definition and its application to generalized Born calculations. *J. Comput. Chem.* **24**, 1348–1356 (2003).
21. G. König, S. Boresch, Hydration free energies of amino acids: Why side chain analog data are not enough. *J. Phys. Chem. B* **113**, 8967–8974 (2009).
22. W. L. Jorgensen, E. M. Duffy, Prediction of drug solubility from structure. *Adv. Drug Deliv. Rev.* **54**, 355–366 (2002).
23. G. König, P. Chiba, G. F. Ecker, Hydrophobic moments as physicochemical descriptors in structure-activity relationship studies of P-glycoprotein inhibitors. *Monatsh. Chem.* **139**, 401–405 (2008).

24. S. Tanizaki, M. Feig, Molecular dynamics simulations of large integral membrane proteins with an implicit membrane model. *J. Phys. Chem. B* **110**, 548–556 (2006).
25. R. M. Venable, A. Krämer, R. W. Pastor, Molecular dynamics simulations of membrane permeability. *Chem. Rev.* **119**, 5954–5997 (2019).
26. J. Witek *et al.*, Rationalization of the membrane permeability differences in a series of analogue cyclic decapeptides. *J. Chem. Inf. Model.* **59**, 294–308 (2019).
27. P. A. Kollman *et al.*, Calculating structures and free energies of complex molecules: Combining molecular mechanics and continuum models. *Acc. Chem. Res.* **33**, 889–897 (2000).
28. S. Genheden, U. Ryde, The MM/PBSA and MM/GBSA methods to estimate ligand-binding affinities. *Expert Opin. Drug Discov.* **10**, 449–461 (2015).
29. G. König, B. R. Brooks, Predicting binding affinities of host-guest systems in the SAMPL3 blind challenge: The performance of relative free energy calculations. *J. Comput. Aided Mol. Des.* **26**, 543–550 (2012).
30. G. König, F. C. Pickard IV, Y. Mei, B. R. Brooks, Predicting hydration free energies with a hybrid QM/MM approach: An evaluation of implicit and explicit solvation models in SAMPL4. *J. Comput. Aided Mol. Des.* **28**, 245–257 (2014).
31. G. König *et al.*, Calculating distribution coefficients based on multi-scale free energy simulations: An evaluation of MM and QM/MM explicit solvent simulations of water-cyclohexane transfer in the SAMPL5 challenge. *J. Comput. Aided Mol. Des.* **30**, 989–1006 (2016).
32. A. P. Spork *et al.*, Lead structures for new antibacterials: Stereocontrolled synthesis of a bioactive muraymycin analogue. *Chemistry* **20**, 15292–15297 (2014).
33. E. Tacconelli *et al.*; WHO Pathogens Priority List Working Group, Discovery, research, and development of new antibiotics: The WHO priority list of antibiotic-resistant bacteria and tuberculosis. *Lancet Infect. Dis.* **18**, 318–327 (2018).
34. R. Leclercq, P. Courvalin, Resistance to macrolides and related antibiotics in *Streptococcus pneumoniae*. *Antimicrob. Agents Chemother.* **46**, 2727–2734 (2002).
35. G. Kahlmeter, D. F. Brown, Harmonization of antimicrobial breakpoints in Europe–can it be achieved? *Clin. Microbiol. Newsl.* **26**, 187 (2004).
36. B. R. Brooks *et al.*, CHARMM: The biomolecular simulation program. *J. Comput. Chem.* **30**, 1545–1614 (2009).
37. B. R. Brooks *et al.*, CHARMM: A program for macromolecular energy, minimization, and dynamics calculations. *J. Comput. Chem.* **4**, 187–217 (1983).
38. J. C. Phillips *et al.*, Scalable molecular dynamics with NAMD. *J. Comput. Chem.* **26**, 1781–1802 (2005).
39. R. B. Best *et al.*, Optimization of the additive CHARMM all-atom protein force field targeting improved sampling of the backbone j, y and side-chain c(1) and c(2) dihedral angles. *J. Chem. Theory Comput.* **8**, 3257–3273 (2012).
40. E. J. Denning, U. D. Priyakumar, L. Nilsson, A. D. Mackerell Jr., Impact of 2′-hydroxyl sampling on the conformational properties of RNA: Update of the CHARMM all-atom additive force field for RNA. *J. Comput. Chem.* **32**, 1929–1943 (2011).
41. K. Vanommeslaeghe *et al.*, CHARMM general force field: A force field for drug-like molecules compatible with the CHARMM all-atom additive biological force fields. *J. Comput. Chem.* **31**, 671–690 (2010).
42. I. Wekselman *et al.*, The ribosomal protein ul22 modulates the shape of the protein exit tunnel. *Structure* **25**, 1233–1241.e3 (2017).
43. Y. Sugita, Y. Okamoto, Replica-exchange molecular dynamics method for protein folding. *Chem. Phys. Lett.* **314**, 141–151 (1999).
44. R. H. Swendsen, J. S. Wang, Replica Monte Carlo simulation of spin glasses. *Phys. Rev. Lett.* **57**, 2607–2609 (1986).
45. G. König, S. Bruckner, S. Boresch, Unorthodox uses of Bennett's acceptance ratio method. *J. Comput. Chem.* **30**, 1712–1718 (2009).
46. G. König, B. R. Brooks, W. Thiel, D. M. York, On the convergence of multi-scale free energy simulations. *Mol. Simul.* **44**, 1062–1081 (2018).
47. S. Metz, J. Kästner, A. A. Sokol, T. W. Keal, P. Sherwood, Chemshell–a modular software package for QM/MM simulations. *Wiley Interdiscip. Rev. Comput. Mol. Sci.* **4**, 101–110 (2014).
48. W. Thiel, MNDO2005 (Version 7.1, Max Planck Institut für Kohlenforschung, Mülheim an der Ruhr, Germany, 2006).
49. P. O. Dral *et al.*, Semiempirical quantum-chemical orthogonalization-corrected methods: Theory, implementation, and parameters. *J. Chem. Theory Comput.* **12**, 1082–1096 (2016).
50. W. Weber, W. Thiel, Orthogonalization corrections for semiempirical methods. *Theor. Chem. Acc.* **103**, 495–506 (2000).
51. S. Grimme, J. Antony, S. Ehrlich, H. Krieg, A consistent and accurate ab initio parametrization of density functional dispersion correction (DFT-D) for the 94 elements H-Pu. *J. Chem. Phys.* **132**, 154104 (2010).
52. TURBOMOLE, Program Package for Electronic Structure Calculations. https://www.turbomole.com. Accessed 24 October 2021.
53. A. D. Becke, Density-functional exchange-energy approximation with correct asymptotic behavior. *Phys. Rev. A Gen. Phys.* **38**, 3098–3100 (1988).
54. F. Weigend, R. Ahlrichs, Balanced basis sets of split valence, triple zeta valence and quadruple zeta valence quality for H to Rn: Design and assessment of accuracy. *Phys. Chem. Chem. Phys.* **7**, 3297–3305 (2005).
55. W. Smith, C. Yong, P. Rodger, Dl_poly: Application to molecular simulation. *Mol. Simul.* **28**, 385–471 (2002).
56. A. D. MacKerell *et al.*, All-atom empirical potential for molecular modeling and dynamics studies of proteins. *J. Phys. Chem. B* **102**, 3586–3616 (1998).
57. T. W. Kim *et al.*, Simple procedures for the construction of a robust and cost-effective cell-free protein synthesis system. *J. Biotechnol.* **126**, 554–561 (2006).
58. H. B. Albada *et al.*, Modulating the activity of short arginine-tryptophan containing antibacterial peptides with N-terminal metallocenoyl groups. *Beilstein J. Org. Chem.* **8**, 1753–1764 (2012).
59. D. Siegmund *et al.*, Benzannulated Re(i)-NHC complexes: Synthesis, photophysical properties and antimicrobial activity. *Dalton Trans.* **46**, 15269–15279 (2017).